Available at www.sciencedirect.com

ScienceDirect

journal homepage: www.elsevier.com/locate/watres

Modelling coupled turbulence – Dissolved oxygen dynamics near the sediment–water interface under wind waves and sea swell

Mathieu Chatelain [a,b,*], *Katell Guizien* [a,b]

[a] *CNRS, UMR 7621, LOBB, Observatoire Océanologique, F-66651 Banyuls/mer, France*
[b] *UPMC Univ Paris 06, UMR 7621, LOBB, Observatoire Océanologique, F-66651 Banyuls/mer, France*

ARTICLE INFO

Article history:
Received 15 July 2009
Received in revised form
30 October 2009
Accepted 7 November 2009
Available online 14 November 2009

Keywords:
Wave boundary layer
Mass transfer
Turbulent diffusion
Unsteady flow
Sediment diagenesis

ABSTRACT

A one-dimensional vertical unsteady numerical model for diffusion-consumption of dissolved oxygen (DO) above and below the sediment–water interface was developed to investigate DO profile dynamics under wind waves and sea swell (high-frequency oscillatory flows with periods ranging from 2 to 30 s). We tested a new approach to modelling DO profiles that coupled an oscillatory turbulent bottom boundary layer model with a Michaelis–Menten based consumption model.

The flow regime controls both the mean value and the fluctuations of the oxygen mass transfer efficiency during a wave cycle, as expressed by the non-dimensional Sherwood number defined with the maximum shear velocity (*Sh*). The Sherwood number was found to be non-dependent on the sediment biogeochemical activity (μ). In the laminar regime, both cycle-averaged and variance of the Sherwood number are very low ($\overline{Sh} < 0.05$, $\mathrm{VAR}(Sh) < 0.1\%$). In the turbulent regime, the cycle-averaged Sherwood number is larger ($\overline{Sh} \approx 0.2$). The Sherwood number also has intra-wave cycle fluctuations that increase with the wave Reynolds number (VAR(*Sh*) up to 30%). Our computations show that DO mass transfer efficiency under high-frequency oscillatory flows in the turbulent regime are water-side controlled by: (a) the diffusion time across the diffusive boundary layer and (b) diffusive boundary layer dynamics during a wave cycle. As a result of these two processes, when the wave period decreases, the *Sh* minimum increases and the *Sh* maximum decreases. $\overline{Sh}$ values vary little, ranging from 0.17 to 0.23. For periods up to 30 s, oxygen penetration depth into the sediment did not show any intra-wave fluctuations. Values for the laminar regime are small ($\leq$1 mm for $\mu = 2000\ \mathrm{g\,m^{-3}\,d^{-1}}$) and decrease when the flow period increases. In the turbulent regime, the oxygen penetration depth reaches values up to five times larger than those in the laminar regime, becoming asymptotic as the maximum shear velocity increases.

1. Introduction

Diffusional mass transfer between bottom sediments and overlying water constitutes an essential coupling for benthic and pelagic ecosystems (Boudreau and Jørgensen, 2001). Transfer of oxygen across the sediment–water interface (SWI) regulates biological and geochemical processes of organic matter degradation in the upper sediment. Vertical oxygen

* *Corresponding author at*: CNRS, UMR 7621, LOBB, Observatoire Océanologique, F-66651 Banyuls/mer, France. Tel.: +33 468 887 394; fax: +33 468 887 395.
E-mail address: chatelain@obs-banyuls.fr (M. Chatelain).
0043-1354/$ – see front matter © 2009 Elsevier Ltd. All rights reserved.
doi:10.1016/j.watres.2009.11.010

mass transfers at the benthic or bottom boundary layer occur in a zone where gradients in physical, chemical and biological properties are sharp. In the water column, solute transport is dominated by turbulent mixing, except within the diffusive boundary layer (DBL) where turbulent diffusivity becomes negligible compared to oxygen molecular diffusion (Gundersen and Jørgensen, 1990). The thickness of the DBL regulates the kinetics of oxygen supply to the benthic organisms: while a thick DBL associated with small steady flow velocities (laminar regime) may be limiting for organisms with high oxygen uptake rates, a thin DBL associated with large steady flow velocities (turbulent regime) results in the highest possible oxygenation (Nakamura and Stefan, 1994; Hondzo, 1998; Steinberger and Hondzo, 1999). In nature, flows are generally turbulent with DBL thicknesses on the order 1–2 mm (Jørgensen and Revsbech, 1985) but they are also more often unsteady. As a consequence, the DBL thickness will fluctuate inducing oxygen profile dynamics (Jørgensen and Des Marais, 1990; Glud et al., 2007). Yet, such dynamics are not instantaneously responding to the hydrodynamic forcing. Transient oxygen profiles were observed in sediment cores immediately after stirring was stopped (Lohse et al., 1996). Numerical simulations have shown that the duration of the transitory regime between two steady states (with and without flow) decreases as both oxygen consumption and flow velocity increase (Higashino et al., 2004).

Amongst unsteady flows, oscillatory flows are of particular interest for the diffusion-consumption of oxygen at the SWI. Periodic flows are frequent in nature as they are linked to surface gravity waves. In the oceans, such flows are the most energetic (Massel, 1996) and they often destabilize the SWI in the nearshore zone (Harris and Coleman, 1998). Surface gravity wave energy is equally distributed between two types characterized by their periods: wind waves and swell (periods from 2 to 30 s) and the diurnal and semi-diurnal tides (periods from 12 to 24 h). In lakes and lagoons, the period range for surface gravity waves is generally restricted to wind waves (periods below 8 s) due to fetch limitations. But other types of oscillatory flows like seiche with longer periods (depending on the basin lengthscale and stratification) can be observed (Proudman, 1953). In 2003, the oxygen profile dynamics linked to periodic bottom layer turbulence under low-frequency waves (lake internal seiching with period of 18 h) was observed for the first time (Lorke et al., 2003). Additionally, the effect of periodic flows (periods ranging from minutes to hours) on oxygen diffusion in the water column was investigated by numerical simulations (Higashino et al., 2003).

The present study examines the effect of wind waves and sea swell (periods ranging from 2 to 30 s) on oxygen dynamics and diffusion at the SWI. Oscillatory flows exhibiting large velocity fluctuations from zero (at flow reversal) to a maximum value (orbital velocity) are associated with these high-frequency gravity waves (Airy, 1845). Near the bed, an oscillatory boundary layer develops which exhibits strong turbulence dynamics with flow relaminarization around reversal (Jensen et al., 1989) and consequently, large DBL thickness fluctuations at the flow periodicity. Under oscillatory flows, the oxygen concentration dynamics may result not only from the DBL thickness value, but also from the DBL dynamics as well. Hence, a new one-dimensional vertical, unsteady numerical model for diffusion-consumption of dissolved oxygen (DO) above and below the SWI was driven by the turbulent diffusivity associated with the wave bottom boundary layer modelled by Guizien et al. (2003). Wind waves and sea swell were described by idealized monochromatic waves to assess the respective influence of the wave period and orbital velocity. The new model was used to examine three fundamental questions about the dynamics of DO distribution under high-frequency waves. First, what are the characteristic time scales of the forcing that drive the intra-wave dynamics of DO? Second, how does the DO mass transfer vary with the wave period and the orbital velocity (mean value and fluctuations during a wave cycle)? And third, to what extent do wind waves and sea swell drive sediment oxygenation?

2. Material and methods

2.1. *Model formulation*

Dissolved oxygen traverses two diffusive boundary layers from the water column into the sediment. The first layer is in the water immediately above the sediment, and the second is in the sediment immediately below the sediment–water interface (Fig. 1).

A one-dimensional vertical (1DV) numerical model of the DO balance in water and sediment is proposed. For the sake of simplicity, we assume a constant porosity of the sediment. Advection due to permeability, bioturbation and bioirrigation in the sediment is neglected. Microbial organic matter degradation occurring in the sediment is taken into account, as well as chemical reactions involving oxygen consumption. Both are modelled by Michaelis–Menten consumption kinetics (House, 2003). Such a mathematical formulation allows a constant consumption when the DO concentration is large (*i.e.* non limiting, zero-order kinetics) and a decreasing consumption when DO concentration approaches zero (first-order kinetics). This formulation is thus consistent with both zero flux and concentration for DO at the lower boundary condition deep in the sediment. Moreover, prescribing a constant consumption near the interface assumes that neither acclimatization nor

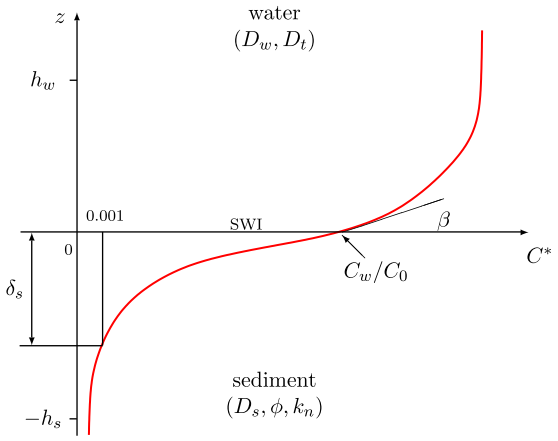

Fig. 1 – Schematic representation of non-dimensional dissolved oxygen concentration profile ($C^* = C/C_0$) at sediment–water interface (SWI).

growth of the respiring community occurs inside a wave cycle. Finally, it is assumed that oxygen consumption can be neglected in the water column. Thus we define:

$$\frac{\partial C^*}{\partial t^*} = \frac{\partial}{\partial z^*}\left(D^* \frac{\partial C^*}{\partial z^*}\right) - \alpha \bullet \frac{\mu^* C^*}{K^*_{O_2} + C^*} \quad (1)$$

where the non-dimensional parameters are

$$C^* = \frac{C}{C_0},\ t^* = \frac{\nu t}{h^2},\ z^* = \frac{z}{h},\ D^* = \frac{D}{\nu},\ \mu^* = \frac{\mu h^2}{\nu C_0},\ K^*_{O_2} = \frac{K_{O_2}}{C_0}. \quad (2)$$

C is the DO concentration, t is the time, z is the vertical coordinate (positive upward), D is the vertical diffusivity, μ is the maximum oxidation rate, K_{O_2} is the oxygen half-saturation constant, and α is a numerical constant ($\alpha = 1$ in sediment and $\alpha = 0$ in water). Reference values are ν the kinematic viscosity in water, C_0 the bulk water concentration, and h a length greater than the sum of the DBL thickness in water and DO penetration depth in sediment.

In sediment, oxygen vertical diffusivity D is equal to the effective diffusivity D_s, which is molecular diffusion corrected for tortuosity. It can be expressed, through Archie's law, as a function of molecular diffusivity and porosity of the sediment (Ullman and Aller, 1982):

$$D_s = \phi^{m-1} D_w \quad (3)$$

where ϕ is the porosity, and m denotes an exponent corresponding to different kinds of sediment ($m = 3$, Manheim and Waterman, 1974). Molecular diffusion D_w for oxygen is assumed constant, using a Schmidt number $Sc = \nu/D_w = 500$ at 20 °C (Denny, 1993).

In water, oxygen vertical diffusivity D is the sum of molecular (D_w) and turbulent (D_t) diffusivities. Using the analogy between momentum and mass transfer, the turbulent diffusivity (D_t) is assumed to be equal to the eddy viscosity (ν_t) in water. The model formulation thus allows time-variations of turbulent diffusivity to account for unsteady hydrodynamics.

Eq. (1) is solved using the implicit finite control volume method of Patankar (1980). The spatial computational domain went from $-h_s$ in the sediment, to h_w in the water column ($h = h_s + h_w$). Two exponential grids were defined with n_s points in sediment and n_w points in water. Each mesh starts at $z = 0$, reading:

$$|z_{i+1} - z_i| = dz_i = sr^i \quad (4)$$

taking (r,s) equals (r_s,s_s) in sediment and (r_w,s_w) in water. The SWI is the first sediment point, located at $z = 0$ ($\alpha = 1$, $D = D_s$). This grid was adopted because it is well adapted to refining the nearbed description of each domain where gradients are sharp. Meshing independence of the computations was studied and showed insensitivity of the results for a resolution that yields $r_s = 1.054$, $s_s = 1 \times 10^{-5}$ ($n_s = 194$) and $r_w = 1.054$, $s_w = 1 \times 10^{-7}$ ($n_w = 320$) for sediment and water, respectively (in Eq. (4)).

Boundary conditions for DO concentration are imposed at the top and the bottom of the calculation domain:

$$\begin{cases} C^* = 0 & \text{at } z^* = -h_s/h \\ C^* = 1 & \text{at } z^* = h_w/h \end{cases} \quad (5)$$

The first condition expresses that all DO reaching the sediment should be utilized within the oxygen penetration depth. The second indicates that at the upper limit of the computational domain the water column is fully mixed and the oxygen concentration equals the bulk water concentration. Bulk DO concentration was arbitrarily set to 10 g m^{-3} (Glud et al., 2003).

As we are dealing with periodic hydrodynamic forcing, a finite number of time steps ($n_t = 360$) is required to define an entire period cycle, and periodic boundary conditions are applied stating $C^*(z,n_t + 1) = C^*(z,1)$. The equilibrium solution is the solution when the maximum DO concentration difference at the same phase during two consecutive cycles was less than a convergence criterion ε. We used $\varepsilon = 10^{-8}$ as the convergence criterion.

2.2. Sediment characteristics and hydrodynamic forcing

This study examines the nearbed dynamics of oxygen mass transport under wave forcing over a smooth bottom, as can be observed in shallow estuaries open to the sea. Porous silty sediment conditions were used (median diameter $d_{50} = 0.002$ cm; bottom roughness $k_n = 0.005$ cm; porosity $\phi = 0.9$). The half-saturation constant for DO is set to a constant value ($K_{O_2} = 0.2$ g m^{-3}, Hao et al., 1983). Two biogeochemical activities were tested: high oxidation rate ($\mu = 2000$ g m^{-3} d^{-1}) and low oxidation rate ($\mu = 50$ g m^{-3} d^{-1}, Higashino et al., 2004). These values correspond to oxygen consumption times in the sediment of 432 s and 4.8 h, respectively.

A linear wave forcing is considered:

$$U(t) = U_w \sin\left(\frac{2\pi t}{T}\right) \quad (6)$$

where T is the leading wave period and U_w is the nearbed orbital velocity.

In order to investigate the effect of oscillating flows (wind waves to sea swell) on DO uptake dynamics, we considered wave orbital velocities ranging from 20 to 200 cm s^{-1} and periods ranging from 2 to 30 s. Virtually, any orbital velocity/period couple can be considered, provided that the wave stability criterion is fullfilled. We excluded some orbital velocity/period couples which are unrealistic as they would correspond to unstable breaking waves. Using a breaking-wave criterion of $H < 0.8\,D$ (where H is the wave height and D is the water depth), the orbital velocity restrictions only applied to waves with periods shorter than 4 s.

Hydrodynamic forcing for the DO model consisted of time-varying eddy viscosity profiles $\nu_t(z, t)$ in the wave boundary layer during a wave cycle. Together with bottom shear stress time series ($\tau(t)$), these were computed using a 1DV bottom boundary layer numerical model dedicated to periodic flow (Guizien et al., 2003), given the bottom roughness k_n. The shear velocity u^* at the bed is then:

$$u^*(t) = \sqrt{\frac{\tau(t)}{\rho}} \quad (7)$$

where ρ denotes the water density.

Fig. 2 shows the time evolution of the shear velocity $u^*(t)$ during a wave cycle for two contrasted wave orbital velocities and the same wave period ($T = 15$ s) to illustrate the laminar

and turbulent regimes. In both regimes, during each half of a wave cycle, shear velocity varies from nearly zero to a maximum u^*_m (not a sine form). As typically seen in oscillatory flows, the shear velocity maximum and minimum are ahead of the wave velocity outside the boundary layer, showing that small velocities (near the bottom) reverse more easily than larger ones (far from the bottom) when the pressure gradient reverses. This phase shift decreases from 45° in the laminar case to about 10° in the fully turbulent regime (Fredsøe and Deigaard, 1992). For the same reason, turbulent diffusivity (not shown) exhibits a phase shift with the outer flow velocity which varies across the boundary layer. The laminar regime is defined by a wave Reynolds number below 320 ($Re_\delta = U_w\delta/\nu$ where $\delta = \sqrt{\nu T/\pi}$ is the wave viscous boundary layer height, Vittori and Verzicco, 1998). In the turbulent regime, the shear velocity value jumps during the acceleration phase, marking the onset of turbulence that occurs after the boundary layer relaminarization around flow reversal (Jensen et al., 1989). In the laminar regime, such a jump is absent (flow remains laminar during the entire wave cycle). The laminar regime ($Re_\delta \leq 320$) is shown in light grey on Fig. 3. For the wave characteristics that were investigated, maximum shear velocities ranged from less than 1 to 8 cm s^{-1}. The sensitivity to the wave period is accentuated when the period is small. The dark grey area indicates breaking wave values on the same figure.

Fig. 4 displays computed turbulent diffusivity profiles every 30° during half a wave cycle in the turbulent regime. Temporal changes in the value of D_t reflect the temporal variations of the viscous sublayer thickness $\delta_\nu(t)$ during a wave cycle (the area where $D_t < \nu = 10^{-2}$ cm^2 s^{-1}). Consequently, the oxygen DBL thickness $\delta_D(t)$ (the area where $D_t < D_w = 2\times10^{-5}$ cm^2 s^{-1}) also shows temporal variations during a wave cycle, ranging from around 5×10^{-3} to 3×10^{-2} cm for $T = 25$ s and $U_w = 120$ cm s^{-1} ($u^*_m = 5$ cm s^{-1}, $Re_\delta = 3385$). It should be noted that the exponential mesh creates a coarser resolution in $\delta_D(t)$ computations for large DBL thicknesses.

2.3. *Model analysis*

Computational results consisted of DO vertical profiles at different phases during a wave cycle. For each DO profile, we defined the interfacial concentration $C_w(t)$, the penetration depth $\delta_s(t)$ (with $C^*(z=\delta_s(t)) = 0.001$) and the dissolved oxygen uptake (DOU(t)) at the SWI (Fig. 1). The latter is evaluated from Fick's first law of diffusion (Berner, 1980):

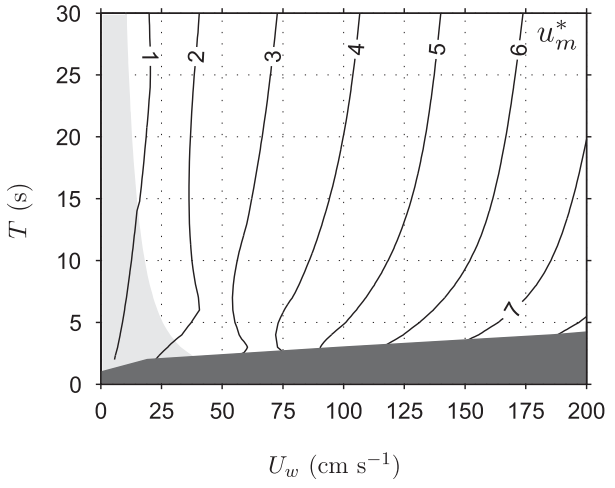

Fig. 3 – Dependence of the maximum shear velocity (u^*_m) on the wave period (T) and orbital velocity (U_w). Dark grey delimits the unstable breaking waves ($H < 0.8\,D$) and light grey delimits the laminar regime ($Re_\delta < 320$).

$$DOU(t) = -D_w\frac{\partial C}{\partial z} = -\frac{D_w C_0}{\beta(t)}. \quad (8)$$

Practically, the instantaneous DOU(t) is computed taking the slope $\beta(t)$ of the DO vertical profile over the three first grid points in water, which height is always much smaller than the DBL thickness. The dimensionless Sherwood number (Sh) is introduced, following Higashino et al. (2003):

$$Sh(t) = \frac{DOU(t)Sc}{u^*_m(C_w(t) - C_0)} \quad (9)$$

where u^*_m is the flow maximum shear velocity. The Sherwood number can be interpreted as a ratio between the effective oxygen transfer rate and turbulent diffusion rate. It thus measures the turbulence efficiency to supply oxygen to the sediment. Following Lorke et al. (2003), we defined a time scale $t_D(t)$ for the oxygen diffusion across the DBL as:

$$t_D(t) = \frac{\delta_D(t)^2}{D_w}. \quad (10)$$

All these time-varying quantities are described by their mean value (indicated by the overline notation) and their

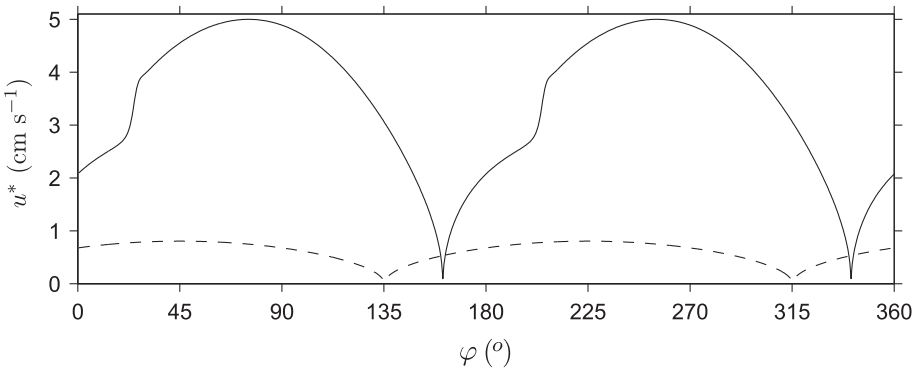

Fig. 2 – Shear velocity (u^*) during a wave cycle for $T = 15$ s, and $u^*_m = 5$ cm s^{-1} (solid line), $u^*_m = 0.8$ cm s^{-1} (dashed line).

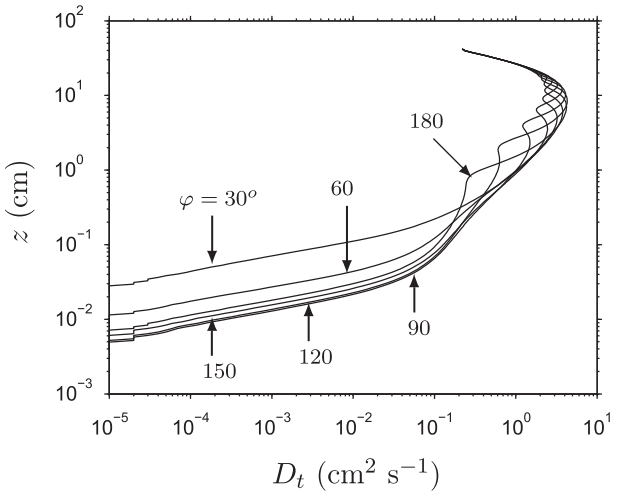

Fig. 4 – Vertical profiles of turbulent diffusivity (D_t) at different wave phases (φ), for $u^*_m = 5$ cm s^{-1} and $T = 25$ s.

variance (VAR(x) = 100 × RMS(x)/$\overline{x}$ in %, where RMS is Root Mean Square) during a wave cycle.

Furthermore, a time scale (t_w) describing the temporal dynamics of the DBL thickness is introduced:

$$t_w(t) = \frac{\delta_D(t)}{\left|\frac{\partial \delta_D}{\partial t}\right|}. \quad (11)$$

This time scale describing the intra-wave DBL dynamics should be compared to the time scale for the establishment of a local DBL. Similar reasoning was adopted by Lorke et al. (2003), where the authors compared relative importance of vertical diffusion versus horizontal advection. When $t_w(t)$ is larger than $t_D(t)$, the DBL thickness varies less rapidly than the time required for the DBL to establish: diffusive fluxes will follow the local DBL thickness fluctuations. Conversely when $t_w(t)$ is smaller than $t_D(t)$, the DBL thickness varies more rapidly than the time required for the DBL to establish: transient diffusive fluxes corresponding to average DBL thickness over the period are simulated.

3. Results

3.1. Intra-wave cycle dynamics

In the laminar regime (shear velocity time series shown on Fig. 2 for $T = 15$ s, $U_w = 10$ cm s^{-1}, $u^*_m = 0.8$ cm s^{-1}, $Re_\delta = 218$), the time required by the oxygen to diffuse through the DBL (t_D) during the wave cycle was very large (≈1.1 days) compared to both the oxygen consumption time in the sediment (t_c) and the wave period (T). The values of t_D were also fairly constant during the wave cycle (data not shown). Consequently, both *DOU* and concentration at the SWI displayed very small and constant values ($DOU = 0.12$ g m^{-2} d^{-1}, $C_w = 0.01$ C_0). The oxygen penetration depth was also very small ($\delta_s = 0.03$ cm). When $t_D >> t_c$, oxygen is consumed more rapidly in the sediment than it diffuses from the water into the sediment: SWI oxygenation is limited by the transfer time through the water DBL.

In the turbulent regime, t_D is much shorter than in the laminar regime, and reaches lower values than t_c. Fig. 5 shows the dynamics during a wave cycle of the parameters u^*, t_D, *DOU* and C_w/C_0 for a 15 s period wave with $U_w = 128$ cm s^{-1} ($u^*_m = 5$ cm s^{-1}, $Re_\delta = 2797$) and the highest oxygen consumption rate in the sediment ($\mu = 2000$ g m^{-3} d^{-1}, $t_c = 432$ s). The oxygen diffusion time through the DBL varied from less than 2 s to about 40 s, with $\overline{t_D} = 10$ s. SWI oxygenation is no longer limited by the transfer time through the DBL, resulting in a much higher *DOU* and interfacial concentration ($\overline{DOU} = 2.1$ g m^{-2} d^{-1}, $\overline{C_w} = 0.86$ C_0), and a higher penetration depth ($\overline{\delta_s} = 0.12$ cm) compared to the laminar regime.

Values of t_D exhibited periodic fluctuations every half a wave cycle (Fig. 5b): it had a maximum around flow reversal and dropped rapidly at the onset of turbulence during flow acceleration. It decreased more gently until the shear velocity reached a maximum (turbulent period labelled θ_1). As the shear velocity decreased, t_D increased slightly during the turbulent period labelled θ_2. Then it increased more rapidly as the bottom boundary layer became laminar during flow deceleration to reach its maximum value again when the outer flow speed is zero. The relaminarization period during which t_D exhibits large values and fluctuations is labelled θ_3. It is interesting to note that due to the phase lagging of the turbulent diffusivity across the bottom boundary layer, the fluctuations of t_D are not phase locked to the fluctuations of the friction velocity.

As a consequence, DO concentrations at the SWI also displayed intra-wave dynamics: the *DOU* at the SWI varied between a minimum and maximum value during each half wave cycle, yielding VAR(*DOU*) = 14% (Fig. 5c). The minimum value of the *DOU* occurs at the end of the relaminarization period θ_3. The *DOU* starts to increase at the laminar–turbulent transition when diffusion time had strongly decreased, reaches a maximum during the turbulent period, and then decreased until the next laminar–turbulent transition. It is noteworthy that during θ_3 (when $t_w < t_D$), the *DOU* decreases steadily without reflecting the large fluctuations of t_D around flow reversal. In contrast, during θ_1 and θ_2, t_w is longer than t_D (bold line on Fig. 5b) and the *DOU* follows the t_D fluctuations. As a result of the *DOU* fluctuations, oxygen concentration at the SWI exhibited similar intra-wave fluctuations, although those were damped (VAR(C_w/C_0) = 1%, Fig. 5d) and delayed compared to the *DOU* fluctuations. Finally, the penetration depth did not display any intra-wave dynamics.

3.2. Effect of the wave period and orbital velocity

Fig. 6 shows the temporal evolutions of t_D, *DOU* and C_w/C_0 during a wave cycle for the same wave period ($T = 15$ s) and three orbital velocities ($U_w = 62$, 128, 195 cm s^{-1}), which correspond to three maximum shear velocities ($u^*_m = 3$, 5, 7 cm s^{-1} respectively) and three Reynolds numbers ($Re_\delta = 1355$, 2797, 4261 resp.). When the maximum shear velocity increases, the minimum value for t_D decreases from 5.3 to 0.7 s since the minimum DBL thickness is imposed by the maximum shear velocity. Moreover, the onset of turbulence occurs at an earlier phase during the accelerating phases of the wave cycle and the duration of period ($\theta_1 + \theta_2$) increases. The duration of the relaminarization period θ_3 decreases from 5 to 2.6 s which limits the laminar DBL development around

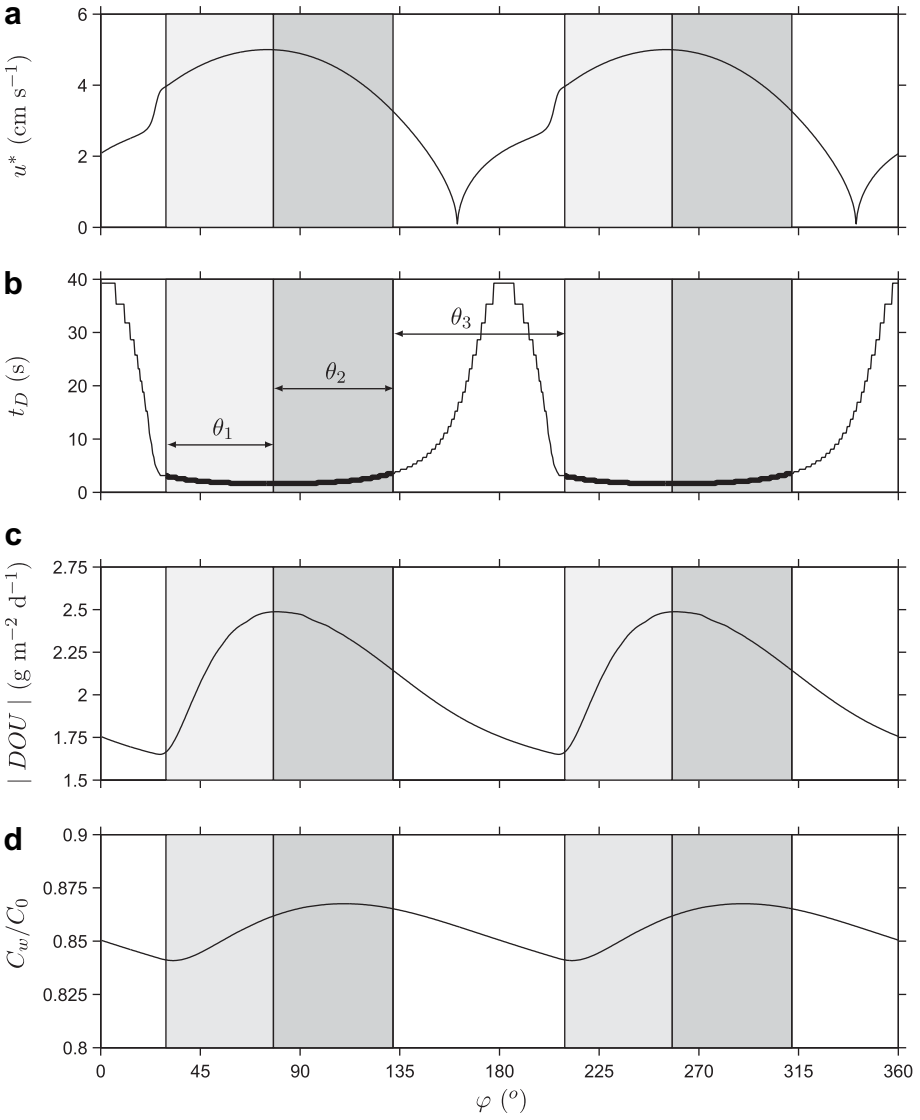

Fig. 5 – Temporal evolution of (a) u^*, (b) t_D, (c) *DOU*, and (d) C_w/C_0 during a wave cycle, for $u^*_m = 5$ cm s^{-1}, $T = 15$ s, and $\mu = 2000$ g m^{-3} d^{-1}. θ_1 (light grey) and θ_2 (dark grey) are turbulent phases, while θ_3 is the relaminarization period.

flow reversal. The maximum values for t_D around flow reversal decreases, although remaining larger than the wave period for the three cases shown on Fig. 6a. As far as *DOU* is concerned (Fig. 6b), when the maximum shear velocity increases, the maximum value of the *DOU* increases and occurs at an earlier phase during the turbulent period. At the same time, the minimum value of the *DOU* decreases, being phase locked to the laminar–turbulent transition. Thus, intra-wave fluctuations of *DOU* and oxygen concentration at the SWI (Fig. 6c) increase with the maximum shear velocity. Since the maximum *DOU* increased more than the minimum *DOU* decreased, cycle-averaged values for *DOU* also tend to increase with the maximum shear velocity, although the values are close: $\overline{DOU}$ ranges from 1.99 to 2.16 g m^{-2} d^{-1}. Cycle-averaged values for the oxygen concentration at the SWI also increase when the shear velocity increases ($\overline{C_w} = 0.78,\ 0.86,\ 0.91\ C_0$ for $u^*_m = 3, 5, 7$ cm s^{-1} respectively). It is interesting to note that while the C_w response to *DOU* fluctuations during a wave cycle is attenuated, its response to changes of cycle-averaged values of *DOU* is amplified.

Fig. 7 shows the temporal evolutions of t_D, *DOU* and C_w/C_0 during a wave cycle for the same maximum shear velocity ($u^*_m = 5$ cm s^{-1}) and three wave periods ($T = 7$, 12, 25 s), which correspond to three Reynolds numbers ($Re_\delta = 1627$, 2404, 3865 resp.). For the three periods, the oxygen diffusion time reached the same minimum value when the shear velocity is maximum, which occurred around the same phase in the three cases: the minimum DBL thickness is imposed by the maximum shear velocity (Fig. 7a). However, as the period increases, not only the time between two flow reversal increases, but also the laminar–turbulent transition occurs at an earlier phase during the accelerating phases of the wave cycle. Consequently, the duration of the turbulent periods ($\theta_1 + \theta_2$) is increased in absolute values and also in proportion of the wave period. When the period increases, the duration of the relaminarization period θ_3 also increases from 2.2 to 5.1 s,

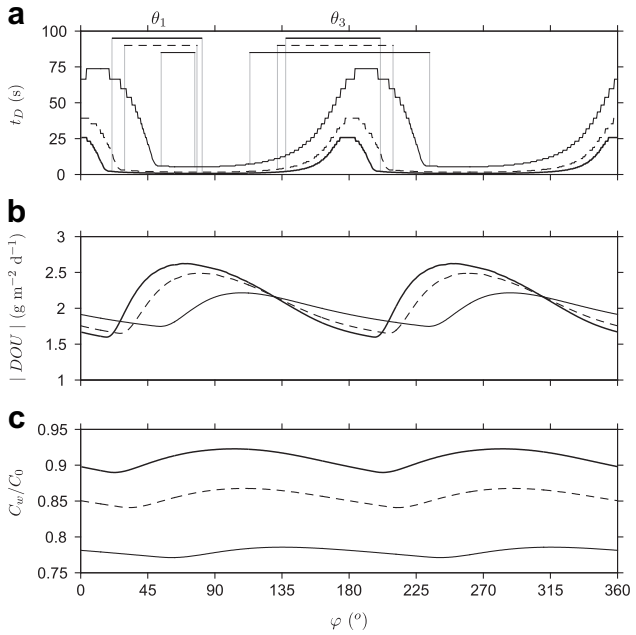

Fig. 6 – Temporal evolution of (a) t_D, (b) *DOU*, and (c) C_w/C_0 during a wave cycle, for $T = 15$ s, $\mu = 2000$ g m^{-3} d^{-1}, and $u^*_m = 3$ cm s^{-1} (solid line), $u^*_m = 5$ cm s^{-1} (dashed line), $u^*_m = 7$ cm s^{-1} (bold line).

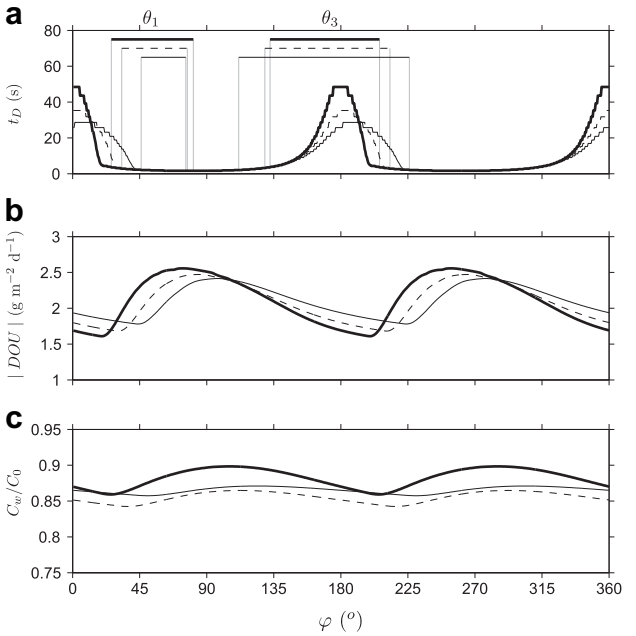

Fig. 7 – Temporal evolution of (a) t_D, (b) *DOU*, and (c) C_w/C_0 during a wave cycle, for $u^*_m = 5$ cm s^{-1}, $\mu = 2000$ g m^{-3} d^{-1}, and $T = 7$ s (solid line), $T = 12$ s (dashed line), $T = 25$ s (bold line).

which facilitates the relaminarization around flow reversal, yielding larger maximum values for t_D. However, in proportion of the wave period, the duration of the period θ_3 decreases. Regarding the *DOU* (Fig. 7b), when the wave period increases, the maximum value of the *DOU* increases while its minimum value decreases. The fluctuations of *DOU* and C_w during the wave cycle (Fig. 7c) thus increase with the period. Although $\overline{DOU}$ values vary little with the wave period ($\overline{DOU}$ ranging from 2.09 to 2.12 g m^{-2} d^{-1}), $\overline{DOU}$ exhibits the minimum value for $T = 12$ s. Cycle-averaged values for the oxygen concentration at the SWI display the same pattern with amplification ($\overline{C_w} = 0.86,\ 0.85,\ 0.88\ C_0$ for $T = 7$, 12 and 25 s respectively).

3.3. *Trends in cycle-averaged DO quantities*

Fig. 8 shows $\overline{DOU}$ and $\overline{C_w}/C_0$ versus the cycle-averaged shear velocity $\overline{u^*}$ in the laminar and the turbulent regimes for two biogeochemical activities. Whatever the flow regime, $\overline{DOU}$ is smaller and $\overline{C_w}/C_0$ is larger for the less active sediment ($\mu = 50$ g m^{-3} d^{-1}) than for the more active sediment. In the laminar regime, $\overline{DOU}$ and $\overline{C_w}/C_0$ increased linearly with the cycle-averaged shear velocity up to 1.6 cm s^{-1}. In the turbulent regime, both quantities reached an asymptote for the largest cycle-averaged shear velocity, up to $\overline{DOU} = 2.15$ g m^{-2} d^{-1} and $\overline{C_w} = 0.9\ C_0$ for $\mu = 2000$ g m^{-3} d^{-1}.

A similar dependence for $\overline{DOU}$, VAR(*DOU*), $\overline{C_w}$ and VAR(C_w) on the wave characteristics was found for high ($\mu = 2000$ g m^{-3} d^{-1}) and low ($\mu = 50$ g m^{-3} d^{-1}) biogeochemical activities in the sediment. The non-dimensional Sherwood number defined by Eq. (9) was used to describe the DO mass transfer at the SWI. It provides a measure of the hydrodynamic efficiency of this mass transfer: the larger the Sherwood number, the lower the maximum shear velocity for the higher oxygen transfer at the SWI. Since the Sherwood number was non-dependent on the biogeochemical activity of the sediment, it summarized the dependency of the DO mass transfer at the SWI on the wave period and the orbital velocity (Fig. 9), and finally on the wave Reynolds number (Fig. 10).

For laminar flow conditions (light grey areas on Fig. 9 and $Re_\delta \leq 320$ on Fig. 10), the large values of t_D significantly hinder the transfer of dissolved oxygen and strongly reduce the presence of oxygen at the SWI, yielding very low non-dimensional mass transfer coefficients on average ($\overline{Sh} < 0.05$). Intra-wave cycle fluctuations are negligible (VAR(Sh) < 0.1%, Figs. 9b and 10b).

As the wave Reynolds number increases, the wave boundary layer becomes turbulent ($Re_\delta > 320$ on Fig. 10). The minimum value of t_D decreases while the duration of the turbulent phases ($\theta_1 + \theta_2$) increases (Fig. 11). Sh has then more time to adjust to the lower values of the minimum of t_D, and its intra-wave fluctuations grow, yielding values up to VAR(Sh) = 30% (Figs. 9b and 10b). Yet, as long as the minimum value of t_D remains longer than the duration of the turbulent part of the wave cycle ($Re_\delta <$ 2050–2500 on Fig. 11), the Sherwood number do not have time to equilibrate with the lower value of t_D and its maximum value is limited by the short duration of the turbulent phase. Consequently, intra-wave fluctuations are transferred to the minimum value of the Sherwood number which decreases rapidly and so does the cycle-averaged value of the Sherwood number (Fig. 10a). As the wave Reynolds number further increases, the minimum value of t_D decreases until reaching shorter values than the period θ_1 ($Re_\delta >$ 2800–3300 on Fig. 11). The maximum value of the Sherwood number increases rapidly, following the decrease of the t_D minimum. At the same

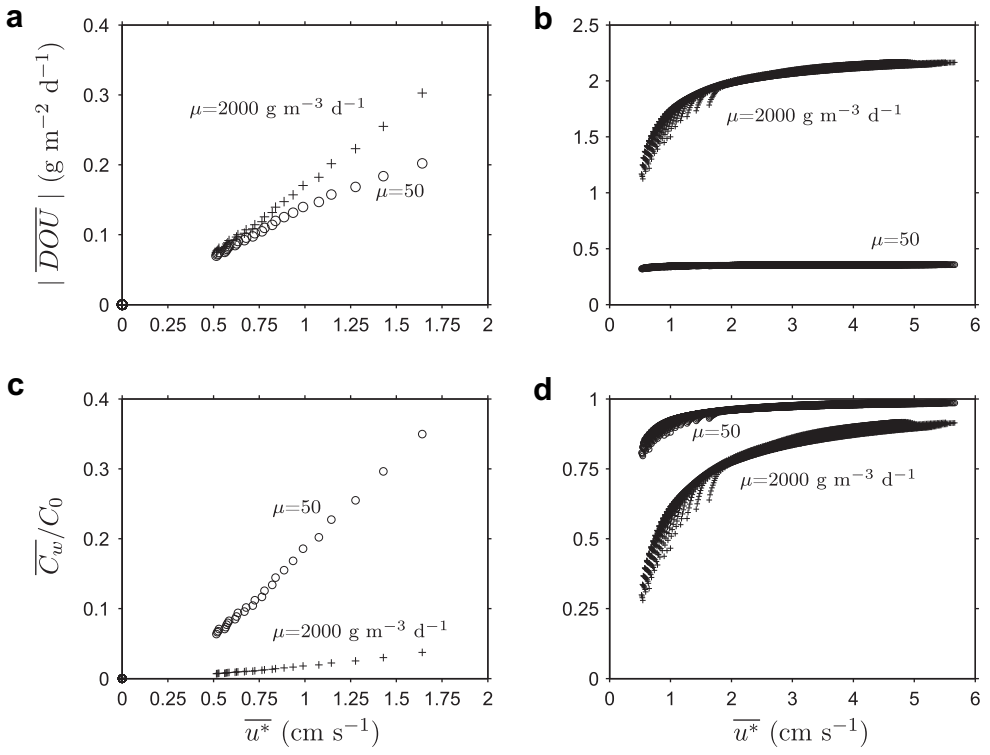

Fig. 8 – Dependences of $\overline{DOU}$ (a,b) and $\overline{C_w}/C_0$ (c,d) on cycle-averaged shear velocity $\overline{u^*}$ for two biogeochemical activities. (a,c) are for the laminar regime ($Re_\delta \leq 320$), (b,d) are for the turbulent regime ($Re_\delta > 320$).

time, the minimum value of the Sherwood number decreases less rapidly due to the shorter duration of the relaminarization period θ_3. As a result, the cycle-averaged value of the Sherwood number increases (Fig. 10a). In summary, the competition between the minimum oxygen diffusion time and the time granted to this rapid diffusion during a wave cycle lead to minimum values of $\overline{Sh}$ for Re_δ between 2050 and 3300 ($10 < T < 15$ s and $80 < U_w < 200$ cm s^{-1} on Fig. 9a). In other words, some sea swells can be less efficient than wind waves (periods below 8 s) for the oxygen mass transfer at the SWI. However, it is noteworthy that overall $\overline{Sh}$ values are very close, ranging from 0.17 to 0.23.

As far as the oxygen penetration depth is concerned, in the laminar regime, it decreased as the wave period increased, whatever the orbital velocity and for the two biogeochemical activities (Fig. 12a). The oxic layer is thin, ranging from 0.38 to 0.79 cm and from 0.02 to 0.06 cm for $\mu = 50$ and $\mu = 2000$ g m^{-3} d^{-1} respectively. When the overlying flow is turbulent, oxygen penetration depth is thicker and strongly depends on the biogeochemical activity in the sediment ($\delta_s = 1.03$ and 0.15 cm for $\mu = 50$ and $\mu = 2000$ g m^{-3} d^{-1} respectively). However, in the turbulent regime, oxygen penetration depth no longer depends on the wave period and reaches an asymptote when shear velocity increases (Fig. 12b). For all the computations, DO penetration depth never showed intra-wave dynamics (*i.e.* VAR(δ_s) = 0).

Finally, the convergence time (t_{st}) of DO profiles from the initial state (where $C^* = 1$ in water and $C^* = 0$ in sediment) to

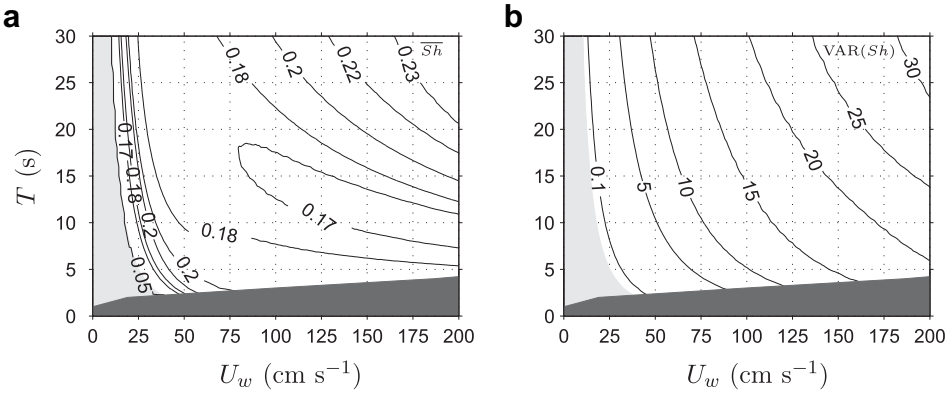

Fig. 9 – Dependences of (a) $\overline{Sh}$, and (b) VAR(Sh) on the wave period (T) and orbital velocity (U_w). Dark grey delimits the unstable breaking waves ($H < 0.8\ D$) and light grey delimits the laminar regime ($Re_\delta < 320$).

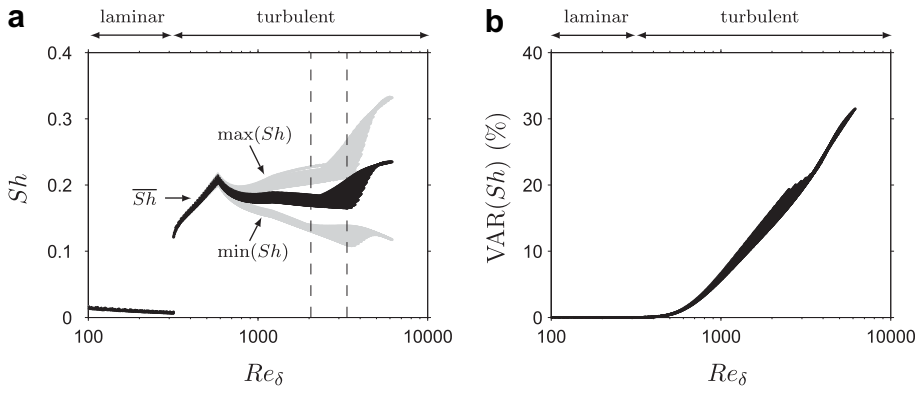

Fig. 10 – Dependences of (a) min(*Sh*), max(*Sh*) and $\overline{Sh}$ and (b) VAR(*Sh*) on the wave Reynolds number (Re_δ). Laminar and turbulent regimes are indicated. Note that max(*Sh*) and min(*Sh*) are represented in grey. The dashed vertical lines delimit the Reynolds numbers range where $\overline{Sh}$ presents a minimum (*see* text).

the equilibrium state was estimated from the calculations (data not shown). In the laminar regime, t_{st} scaled from around 20–108 h and from around 20–92 h when biogeochemical consumption was low ($\mu = 50\ g\,m^{-3}\,d^{-1}$) and high ($\mu = 2000\ g\,m^{-3}\,d^{-1}$), respectively. Time to reach equilibrium state is shorter when the flow is turbulent (less than 15 h). For the less active sediment, t_{st} varied little (between 11 and 13 h) with the wave period or orbital velocity. For the more active sediment, t_{st} ranged from 1 to 15 h, and fastest convergence was obtained for the higher Reynolds number.

4. Discussion

4.1. *Comparison with steady flows and low-frequency flows*

The present study indicates that under waves, the flow regime of the boundary layer (laminar or turbulent, defined by the wave Reynolds number Re_δ for oscillatory flows) controls both the *DOU* and the oxygen concentration at the SWI. In the turbulent regime, our results further shows that an increase in the shear velocity also causes an increase of the *DOU* inside the wave cycle.

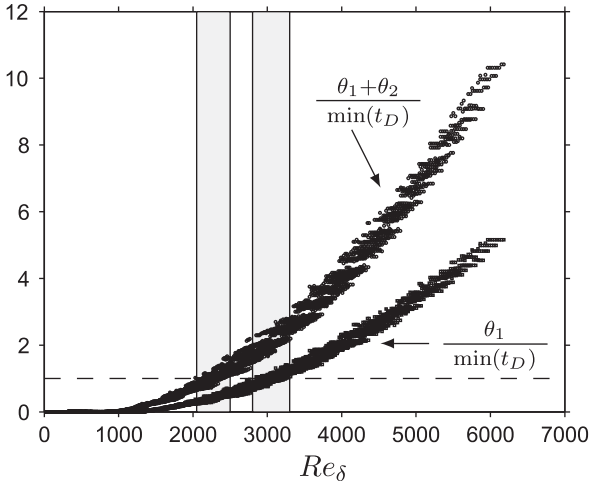

Fig. 11 – Dependences of the ratios ($\theta_1 + \theta_2$)/min(t_D) and θ_1/min(t_D) on the wave Reynolds number (Re_δ). Light grey areas indicate the ranges of Reynolds number where the ratios become larger than 1 (horizontal dashed line).

These results are qualitatively in agreement with previous experimental studies on steady flows, which showed an increase of the oxygen uptake with the flow shear velocity and thus with the Reynolds number (Booij et al., 1994; Mackenthun and Stefan, 1998; Steinberger and Hondzo, 1999; Tengberg et al., 2004). These results were obtained for various sediment types (natural and artificial), but no indication of the sediment biogeochemical activities were given. Consequently, direct comparison of our results with previous published experimental work cannot be quantitative. To our knowledge, the only study which can be used for a quantitative comparison is the numerical study by Higashino et al. (2004). For $\overline{u^*} = 1$ cm s^{-1} and $\mu = 2000\ g\,m^{-3}\,d^{-1}$, *DOU* levels are similar for steady and unsteady flows ($DOU = 1.7\ g\,m^{-2}\,d^{-1}$), but the oxygenation at the interface is greater in the case of steady flows ($C_w = 0.75\ C_0$ while $C_w = 0.6\ C_0$ for unsteady flows). The cycle-averaged Sherwood number reached $Sh = 0.39$ for the steady flow, while it reached $\overline{Sh} = 0.20$ for the unsteady wave. In summary, for the same mean shear velocity, high-frequency flows appears less efficient on average than steady current for the oxygen mass transfer at the SWI.

This conclusion is in contradiction with previous published work by Higashino et al. (2003). The authors extrapolated their results on low-frequency flows (periods ranging from 10 s to 10 h) to state that when the wave period tends to zero, the cycle-averaged Sherwood number should approach a maximum corresponding to the Sherwood number value for steady flow conditions at the shear velocity maximum. Indeed, in their study, the Sherwood number maximum value was set by the shear velocity maximum, while only the intra-wave minimum value of the Sherwood number increased as the wave period decrease from 10 h to 10 s. In our computations, both the minimum and the maximum values of the Sherwood number vary with the wave Reynolds number, leading to a more complex dependence of $\overline{Sh}$ (Fig. 10). This complex dependence comes from the

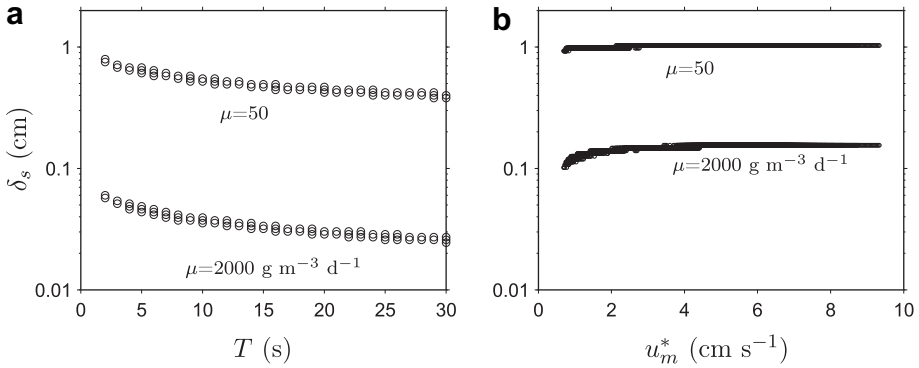

Fig. 12 – Dependences of the penetration depth (δ_s) on (a) the wave period (T) for the laminar regime ($Re_\delta \leq 320$), and (b) the maximum shear velocity (u^*_m) for the turbulent regime ($Re_\delta > 320$), and the two biogeochemical activities tested.

competition between the minimum oxygen diffusion time and the time granted to this rapid diffusion during a wave cycle, which are of the same order of magnitude for high-frequency flows. Thus it appears important to account for the dependency of the phase at which the laminar–turbulent transition occurs on the wave Reynolds number (Jensen et al., 1989). This feature is well reproduced by the transitional boundary layer model we used to compute the unsteady diffusive forcing (Guizien et al., 2003) while it is not using a time-varying water diffusivity derived from a steady-state parameterization (Dade, 1993). Hence, the assumption made by Higashino et al. (2003) may be valid for slowly-varying flows but not for high-frequency flows.

Our results also showed that in the turbulent regime, the periodic fluctuations of the DO concentration around the SWI under oscillatory forcing are not phase locked with the DBL fluctuations, as a result of the vertical phase lagging of diffusivity. These features were previously observed on a lake internal seiching with a period of 18 h (Lorke et al., 2003).

It is also interesting to note that the cycle-averaged Sherwood number computed in Higashino et al. (2003) for a periodic flow ($T = 20$ s, $\overline{Sh} = 0.5$) was larger than the value obtained by Higashino et al. (2004) for a steady flow at the same maximum shear velocity ($\overline{Sh} = 0.39$). We argue that $\overline{Sh}$ values were overestimated by Higashino et al. (2003) probably because the interfacial oxygen concentration was assumed as a constant.

In the present study, sediment oxygen consumption was modelled using a Michaelis–Menten kinetic formulation. This formulation assumes explicitly that no acclimatization of the respiring community occurs during a wave cycle. Such absence of respiration acclimatization should be tested experimentally as a function of the wave period, for instance with high resolution DO measurements. Although promising results have accompanied the development of optical methods for oxygen concentration profiling (Revsbech et al., 1998), faster oxygen profiles measurements are still required to observe the high-frequency fluctuations of the dissolved oxygen uptake related to the high-frequency wave turbulence. Indeed, turbulence and DO concentrations should be measured simultaneously at high-frequency to evaluate the tested model design and the biological interpretations of the mass transfer dynamics at the SWI under periodic waves. The novel non-invasive eddy correlation technique (Berg et al., 2003) might be a solution, using phase-averaging to tackle the requirement for a large integration time.

4.2. *Relevancy for biological systems*

Three processes, all with different time scales, interplay to drive the oxygen dynamics during wave period: (1) the oxygen consumption in the sediment, (2) the oxygen diffusion across the DBL, and (3) the DBL periodic dynamics. The relative importance of the first two processes was discussed by Higashino et al. (2004) for steady flows. When the oxygen diffusion time across the DBL is much larger than the oxygen consumption time in the sediment, the SWI oxygenation is limited by the oxygen supply, leading to low values for the *DOU* and C_w (laminar regime). Conversely in the turbulent regime, the oxygen diffusion time across the DBL is strongly reduced and SWI oxygenation is then scaled by the oxygen consumption in the sediment. In the case of unsteady wave forcing, the DBL periodicity whose time scale is the wave period will interfere with the oxygen consumption and diffusion. For high-frequency waves with periods up to 30 s, the sediment oxygen consumption time will always remain longer than the wave period. Thus, any periodic fluctuation disappears rapidly in the sediment. In the turbulent regime, the oxygen diffusion time can reach shorter values than the wave period: every half a wave period, the oxygen diffusion time falls during the turbulent phase. Briefly put, as long as the minimum value of t_D remains lower than the duration of the turbulent part of the wave cycle, oxygen concentration will have time to equilibrate with the low values of t_D, and *DOU* will fluctuate each half a wave period: fluctuations increase with the wave Reynolds number.

Oxygen near the SWI is essential for both biological production and decomposition processes. Oxygen concentration is a regulating mechanism for benthic community complexity (Llansó, 1992), for regeneration of nutrients (Rahm and Svensson, 1989), and it also constrains chemical (Cai and Sayles, 1996) and biological (House, 2003) reactions. Hypoxic conditions ($C < 2$ ml l$^{-1} \approx 2.4$ g m^{-3}) may significantly disturb the growth and metabolism of benthic organisms and can cause mass mortality of marine animals, resulting in benthic defaunation and fish community decline (Diaz and Rosenberg, 1995, and references herein). In the laminar regime, the transfer

of DO is strongly impeded by the thickness of the DBL and the interfacial concentration reaches hypoxic levels ($C_w = 0.1$–0.2 $C_0 = 1$–$2\ g\ m^{-3}$). Over the range of wave conditions we tested, the laminar regime corresponds to orbital velocities lower than $40\ cm\ s^{-1}$ for the periods below 5 s and orbital velocities lower than $15\ cm\ s^{-1}$ for periods up to 25 s. For the smallest periods corresponding to building wind waves (below 5 s), the wave height is also generally small and the laminar regime should be the most frequent regime in the bottom boundary layer, except for very shallow conditions (less than half a meter of water) in closed basins like small lakes or lagoons.

As the wave period increases (when the wind fetch is larger), the laminar regime would become rarer: for instance, for a wave period of 8 s over 10 m water depth, the wave bottom boundary layer would be turbulent for a wave height H larger than 0.3 m. For $H = 1.6$ m, orbital velocities reach $60\ cm\ s^{-1}$ ($\overline{u^*} = 2.1\ cm\ s^{-1}$), and yields on average a high SWI oxygenation ($\overline{C_w} \approx 0.8\ C_0$) due to a large flux ($\overline{DOU} > 2\ g\ m^{-2}\ d^{-1}$). Such wave conditions are frequently observed at sea (about 50% of the time on the French Atlantic coast, Butel et al., 2002) and will promote a high oxygenation of the SWI most of the time. Additionally, DO profiles respond to the flow within a few hours. Even short events of wind waves or sea swell may notably stimulate shallow sediment oxygenation and oxygen exchange across the SWI. Besides, it may be estimated that waves promotes a high sediment oxygenation more frequently than steady currents. Indeed, after Higashino et al. (2004), reaching $C_w \approx 0.8\ C_0$ under a steady flow requires a lower oxygen flux $\overline{DOU} = 1.8\ g\ m^{-2}\ d^{-1}$ associated with a lower shear velocity of $1.35\ cm\ s^{-1}$. Such steady shear velocity values correspond to a current speed of $30\ cm\ s^{-1}$ at 1 m above a smooth bed. Even the most energetic tidal flow will not have such values more than 50% of the time.

Furthermore, oxygen concentration at the SWI can be dynamically driven by periodic fluctuations of the DBL thickness under wind waves and sea swell. Yet the amplitude of these fluctuations during a wave cycle may not be sufficient to stress the benthic macrofauna (around 1% for C_w/C_0 for instance). In the sediment, periodic fluctuations vanish rapidly and oxygen penetration depth largely depends on the oxygen consumption in the sediment. This sediment inertia is explained by the larger oxygen consumption time (t_c) in the sediment compared to the DBL dynamics time scale during a wave period (t_w). For flows having periods of hours (tides, inertial waves, etc.) or smaller consumption time (*i.e.* smaller C_0, for instance), it can be expected that t_w will reach values comparable to or even larger than t_c. In such cases, periodic fluctuations of oxygen concentration may be expected not only in the overlying water but also in the sediment. However, the fluctuation range as well as the cycle-averaged value are not trivial to extrapolate since a strong coupling between the DBL dynamics, the oxygen diffusion across the DBL, and the oxygen consumption in the sediment is likely to exist when characteristic time scales (t_D, t_c and t_w) have similar orders of magnitude.

5. Conclusions

The response of dissolved oxygen profiles to a wide range of wind waves to sea swell conditions over a smooth bottom was studied. Oxygen diffusion time across the diffusive boundary layer (t_D), dissolved oxygen uptake (*DOU*), interfacial concentration (C_w), Sherwood number (*Sh*), and oxygen penetration depth (δ_s) were described by their cycle-averaged value and their standard deviation during a wave cycle.

- As in steady flows, the flow regime (turbulent or laminar) controls both the *DOU* and the oxygen concentration at the SWI. In the laminar regime, oxygen mass transfer efficiency is strongly impeded, yielding small and constant *DOU*, C_w and δ_s values during the wave cycle. In the turbulent regime (frequent under waves), oxygen supply to the sediment is no longer limited resulting in higher values for $\overline{DOU}$, $\overline{C_w/C_0}$ and δ_s (Figs. 8 and 12).
- In the turbulent regime, *DOU* and C_w exhibit periodic fluctuations in response to the unsteady DBL thickness: their dynamics were water-side controlled by the ratio between (a) the oxygen diffusion time across the DBL (t_D), and (b) a time scale of the temporal dynamics of the DBL thickness (t_w). When $t_w(t)$ was smaller than $t_D(t)$, the DBL thickness varied more rapidly than the time required for diffusive flux to establish: diffusive flux corresponded to the average DBL thickness over a period. Conversely, when $t_w(t)$ was larger than $t_D(t)$, diffusive flux followed the local DBL thickness fluctuations (Fig. 5). Unsteady properties of the overlying high-frequency flow were never transmitted deeply into the sediment ($VAR(\delta_s) = 0$).
- Dependence of the oxygen mass transfer efficiency on the wave period and the orbital velocity and finally on the wave Reynolds number are summarized by the dimensionless Sherwood number trends. The latter was found non-dependent on the sediment biogeochemical activity. The cycle-averaged Sherwood values ($\overline{Sh}$) vary little, ranging from 0.17 to 0.23. Minimum values result from the competition between the minimum oxygen diffusion time and the time granted to this rapid diffusion during a wave cycle (Re_δ between 2050 and 3500, Fig. 10a). They correspond to sea swells having periods ranging from 10 to 15 s (Fig. 9a). Intra-wave fluctuations VAR(*Sh*) increase as both wave period and orbital velocity (*i.e.* Reynolds number) increase, ranging from 0.1% in the laminar regime to 30% in the turbulent regime (Figs. 9b and 10b). Finally, although a high-frequency wave appears less efficient than a steady current at the same mean shear velocity for the oxygen mass transfer, wind waves and sea swell are likely to promote high sediment oxygenation more frequently than steady currents.

Acknowledgements

We would like to thank Jennifer Guarini for correcting the English and for commenting on an earlier version of this paper. The critical remarks of two anonymous reviewers helped to improve the manuscript. This work is a partial fulfillment of the PhD Thesis of Mathieu Chatelain who is supported by a doctoral fellowship from the French National Center for Scientific Research (CNRS) and by

founds from the Research Program VASIREMI (ANR-06-BLAN-0393-01).

Appendix A. Supplementary material

Supplementary data associated with this article can be found, in the online version, at doi:10.1016/j.watres.2009.11.010.

REFERENCES

Airy, G.B., 1845. Tides and Waves. Encyclopaedia Metropolitana.

Berg, P., Røy, H., Janssen, F., Meyer, V., Jørgensen, B.B., Hüttel, M., de Beer, D., 2003. Oxygen uptake by aquatic sediments measured with a novel non-invasive eddy-correlation technique. Marine Ecology Progress Series 261 (1), 75–83.

Berner, R.A., 1980. Early Diagenesis: a Theoretical Approach. Princeton University Press, Princeton.

Booij, K., Sundby, B., Helder, W., 1994. Measuring the flux of oxygen to a muddy sediment with a cylindrical microcosm. Netherlands Journal of Sea Research 32, 1–11.

Boudreau, B.P., Jørgensen, B.B., 2001. The Benthic Boundary Layer: Transport Processes and Biogeochemistry. Oxford University Press, Oxford.

Butel, R., Dupuis, H., Bonneton, P., 2002. Spatial variability of wave conditions on the French Atlantic coast using in-situ data. In: Proc, vol. 2. ICS.

Cai, W.-J., Sayles, F.L., 1996. Oxygen penetration depths and fluxes in marine sediments. Marine Chemistry 52 (2), 123–131.

Dade, W., 1993. Near-bed turbulence and hydrodynamic control of diffusional mass transfer at the sea floor. Limnology and Oceanography 38 (1), 52–69.

Denny, M.W., 1993. Air and Water: the Biology and Physics of Life's Media. Princeton University Press, Princeton.

Diaz, R.J., Rosenberg, R., 1995. Marine benthic hypoxia: a review of its ecological effects and the behavioural responses of benthic macrofauna. Oceanographic Marine Biology Annual Review 33 (1), 245–303.

Fredsøe, J., Deigaard, R., 1992. Mechanics of Coastal Sediment Transport. Advanced Series on Ocean Engineering, vol. 3. World Scientific.

Glud, R.N., Berg, P., Fossing, H., Jørgensen, B.B., 2007. Effect of the diffusive boundary layer on benthic mineralization and O2 distribution: a theoretical model analysis. Limnology and Oceanography 52 (2), 547–557.

Glud, R.N., Gundersen, J.K., Røy, H., Jørgensen, B.B., 2003. Seasonal dynamics of benthic oxygen uptake in a semienclosed bay: importance of diffusion and faunal activity. Limnology and Oceanography 48 (3), 1265–1276.

Guizien, K., Dohmen-Janssen, M., Vittori, G., 2003. 1DV bottom boundary layer modeling under combined wave and current: turbulent separation and phase lag effects. Journal of Geophysical Research 108 (C1), 3016. doi:10.1029/2001JC001292.

Gundersen, J.K., Jørgensen, B.B., 1990. Microstructure of diffusive boundary layers and the oxygen uptake of the sea floor. Nature 345 (6276), 604–607.

Hao, O.F., Richard, M.G., Jenkins, D., Blanch, H.W., 1983. The half-saturation coefficient for dissolved oxygen: a dynamic method for its determination and its effect on dual species competition. Biotechnology and Bioengineering 25 (1), 403–416.

Harris, P.T., Coleman, R., 1998. Estimating global shelf sediment mobility due to swell waves. Marine Geology 150 (1–4), 171–177.

Higashino, M., Gantzer, C.J., Stefan, H.G., 2004. Unsteady diffusional mass transfer at the sediment/water interface: theory and significance for SOD measurement. Water Research 38 (1), 1–12.

Higashino, M., Stefan, H.G., Gantzer, C.J., 2003. Periodic diffusional mass transfer near sediment/water interface: theory. Journal of Environmental Engineering 129 (5), 447–455.

Hondzo, M., 1998. Dissolved oxygen transfer at the sediment-water interface in a turbulent flow. Water Resources Research 34 (12), 3525–3533.

House, W.A., 2003. Factors influencing the extent and development of the oxic zone in sediments. Biogeochemistry 63 (3), 317–334.

Jensen, B.L., Sumer, B.M., Fredsøe, J., 1989. Turbulent oscillatory boundary layers at high Reynolds numbers. Journal of Fluid Mechanics 206 (1), 265–297.

Jørgensen, B.B., Des Marais, D.J., 1990. The diffusive boundary layer of sediments: oxygen microgradients over a microbial mat. Limnology and Oceanography 35 (6), 1343–1355.

Jørgensen, B.B., Revsbech, N.P., 1985. Diffusive boundary layers and the oxygen uptake of sediments and detritus. Limnology and Oceanography 30 (1), 111–122.

Llansó, R.J., 1992. Effects of hypoxia on estuarine benthos: the lower Rappahannock river (Chesapeake Bay), a case study. Estuarine, Coastal and Shelf Science 35 (5), 491–515.

Lohse, L., Epping, E.H., Helder, W., Van Raaphorst, W., 1996. Oxygen pore water profiles in continental shelf sediments of the North Sea: turbulent versus molecular diffusion. Marine Ecology Progress Series 145 (1), 63–75.

Lorke, A., Müller, B., Maerki, M., Wüest, A., 2003. Breathing sediments: the control of diffusive transport across the sediment-water interface by periodic boundary-layer turbulence. Limnology and Oceanography 48 (6), 2077–2085.

Mackenthun, A.A., Stefan, H.G., 1998. Effect of flow velocity on sediment oxygen demand: experiments. Journal of Environmental Engineering 124, 222–230.

Manheim, F.T., Waterman, L.S., 1974. Diffusimetry (diffusion constant estimation) on sediment cores by resistivity probe. In: Initial Reports of Deep-Sea Drilling Project, vol. 22(1), pp. 663–670.

Massel, S.R., 1996. Ocean Surface Waves. Their Physics and Prediction. World Scientific.

Nakamura, Y., Stefan, H.G., 1994. Effect of flow velocity on sediment oxygen demand: theory. Journal of Environmental Engineering 120 (5), 996–1016.

Patankar, S.V., 1980. Numerical Heat Transfer and Fluid Flow. MacGraw-Hill, New-York.

Proudman, J., 1953. Dynamical Oceanography. Methuen London and Wiley, New-York.

Rahm, L., Svensson, U., 1989. On the mass transfer properties of the benthic boundary layer with an application to oxygen fluxes. Netherlands Journal of Sea Research 24 (1), 27–35.

Revsbech, N.P., Nielsen, L.P., Ramsing, N.B., 1998. A novel microsensor for determination of apparent diffusivity in sediments. Limnology and Oceanography 43 (5), 986–992.

Steinberger, N., Hondzo, M., 1999. Diffusional mass transfer at sediment-water interface. Journal of Environmental Engineering 125 (2), 192–200.

Tengberg, A., Stahl, H., Gust, G., Muller, V., Arning, U., Andersson, H., Hall, P.O.J., 2004. Intercalibration of benthic fluxes chambers I. Accuracy of flux measurements and influence of chamber hydrodynamics. Progress in Oceanography 60, 1–28.

Ullman, W.J., Aller, R.C., 1982. Diffusion coefficients in nearshore marine sediments. Limnology and Oceanography 27 (3), 552–556.

Vittori, G., Verzicco, R., 1998. Direct simulation of transition in an oscillatory boundary layer. Journal of Fluid Mechanics 37, 207–232.